Nano Research 2013, 6(7): 547–561
DOI 10.1007/s12274-013-0333-7
Review Article
ISSN 1998-0124
CN 11-5974/O4

Sodium lanthanide fluoride core–shell nanocrystals: A general perspective on epitaxial shell growth

Noah J. J. Johnson and Frank C. J. M. van Veggel (✉)

Department of Chemistry, University of Victoria, P.O. Box 3065, Victoria, British Columbia, Canada, V8W 3V6

Received: 17 April 2013
Revised: 16 May 2013
Accepted: 19 May 2013

KEYWORDS
upconverting nanocrystals,
core–shell,
lanthanides,
epitaxy

ABSTRACT

Understanding the structural characteristics and growth mechanism(s) are essential for generating core–shell nano-heterostructures with distinctive properties. Especially in lanthanide-based nanocrystals, rational design of the core–shell composition can be utilized to enhance/tune the optical properties of the final nanostructure, or can be used to integrate multiple functional applications (e.g., luminescent/magnetic). In this article, we review the progress in our current understanding of the epitaxial shell growth in sodium lanthanide fluoride ($NaLnF_4$) nanocrystals. In order to understand epitaxial shell growth the core nanocrystals have to be uniform, and to date the synthesis of high quality near uniform size/shape dispersion controlled synthesis of lanthanide-based nanocrystals has been achieved mainly with this class of nanocrystals. The progress in core–shell synthesis and the epitaxial shell growth mechanism in this class of nanocrystals ($NaLnF_4$) are reviewed, and a general perspective is provided on the core–shell morphology based on different characterization techniques. While there has been tremendous progress in studying the impact of core–shell structures in various functional applications, this review also highlights, in our view, the still limited understanding of ways to control the core–shell morphology and it emphasizes some important, unanswered questions that remain to be addressed to maximize their performance.

1 Introduction

The ability to manipulate the properties of colloidal nanocrystals by epitaxial growth of closely lattice matched material(s) to generate core–shell structures has widely been explored in almost every class of nanomaterial applications [1]. The unique advantage with core–shell nanocrystals is that it allows for integration of two or more functions in one single nanostructure, while spatially isolating the core from the surrounding (e.g., solvents and surface ligands). This spatial separation of the core has had tremendous impact, especially on luminescent nanocrystals, and (epitaxial) shell growth is well known to enhance the luminescence efficiency [2, 3]. The surface-induced solvent and ligand quenching result in low luminescence

Address correspondence to fvv@uvic.ca

efficiency of the core nanocrystals, and the epitaxial shell shields the core from these detrimental effects. In lanthanide-based nanocrystals the luminescence arises from selectively doped lanthanide ions (through their intra-4f transitions) within the nanocrystal matrix and is not a quantum size effect as in semiconductor quantum dots. In spite of the fact that the emissive centers are the dopant ions within the nanocrystal matrix, surface quenching still greatly decreases the luminescence efficiency. The luminescence quenching can directly be attributed to the high energy vibrational modes of the surface ligands and solvents (often water) that, by non-radiative processes, very efficiently quench the emissive ions that are at or near the surface of the nanocrystals. The first evidence of luminescence enhancement by shell growth in lanthanide-based nanocrystals was demonstrated by Haase and co-workers on a green-emitting terbium (Tb^{3+}) doped cerium phosphate ($CePO_4$) core with a lanthanum phosphate ($LaPO_4$) shell [4]. The now widely used core–shell strategy of growing a shell of the same core composition without the dopant ions was then demonstrated by Stouwdam and van Veggel in lanthanum fluoride (LaF_3) nanocrystals with either europium (Eu^{3+}) or terbium (Tb^{3+}) doped in the core with a shell of undoped LaF_3 [5].

One important class of lanthanide-based nanocrystals that has attracted major research focus in recent years is the upconverting nanocrystals [6]. On selective doping of lanthanide ions, these nanocrystals sequentially absorb two or more lower-energy photons and subsequently emit a higher-energy photon, termed as upconversion [7]. This is thus a non-linear process. To date, the bulk form of β-$NaYF_4$ (sodium yttrium fluoride) is known to be the most efficient host matrix for this upconversion process [8, 9]. In nanocrystalline β-$NaYF_4$ structures the increased surface to volume ratio results in enhanced surface quenching and the luminescence efficiency is greatly reduced compared to the bulk structure [10]. To enhance the upconversion efficiency there has been a great deal of interest in core–shell structures with this class of nanomaterials.

In this review, a general perspective on the advances in core–shell synthesis, applications, and characterization of core–shell composition in $NaLnF_4$ nanocrystals is presented. In section 2, we discuss the structural motif of an ideal (perfect) core–shell structure, homo/hetero-epitaxial core–shell structures, and their advantages. Discussion of the different epitaxial shell growth techniques and the shell growth mechanism is then presented in section 3. Subsequently, the characterization techniques to establish the core–shell structure are reviewed in section 4. Finally, in section 5 we remark on some important questions from known examples and highlight the need for further explorations and insights towards designing ideal (perfect) core–shell structures in this class of nanomaterials.

2 Structural composition of core–shell structures, and their functional advantages

2.1 Structural motif of a core–shell nanocrystal

Generally, in epitaxial growth the shell material, with a closely matched lattice structure and composition to that of the core, deposits on the core nanocrystals generating core–shell structures. The final core–shell morphology can be distinguished as either centrosymmetric or non-centrosymmetric structures as shown in Scheme 1. In centrosymmetric structures the deposited shell is equally thick around the core, which is thus an ideal (perfect) core–shell structure. However, in non-ideal cases, beyond a few monolayer shell growth (a "critical" thickness), the interfacial strain induced by the (small) lattice mismatch of the core and shell relaxes and results in defective shell

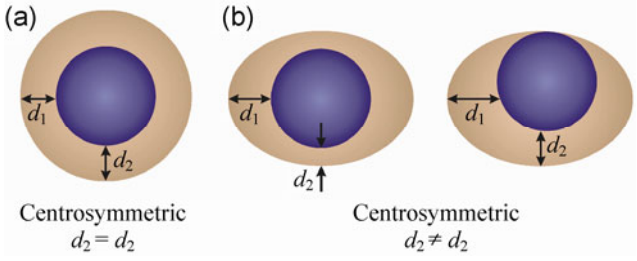

Scheme 1 Illustration of structural composition of core–shell nanocrystals: (a) centrosymmetric ideal core–shell structures where the shell thickness is the same around the core radially in all directions; (b) non-centrosymmetric core–shell anisotropic structures with uneven distribution of the shell around the core, with either complete asymmetric coverage of the core or partially exposed core.

growth generating anisotropic non-centrosymmetric structures [11].

In case of luminescent upconverting nanocrystals an ideal core–shell structure where the shell equally protects the core radially on all sides should provide enhanced upconversion efficiency compared to the core and the other non-centrosymmetric structures. The luminescence quenching by surface ligands and solvents is distant dependent (through the Förster mechanism) and the spatial screening of the core by the shell equally on all sides (centrosymmetric) is thus needed for enhancing the upconversion efficiency. In this regard, a deeper understanding of the shell growth mechanism and in-depth characterization of the core–shell structures are vital towards making progress in designing ideal core–shell nanostructures.

2.2 Classification of core–shell nanocrystals based on their structural composition

The core–shell structures investigated to date in the $NaLnF_4$ class of nanostructures can be classified into two distinct classes, based on the distribution of dopant ions within the core and the shell (class-1), or based on the host matrix composition of the core and the shell (class-2). The class-1 structures can further be classified into two types. In type-1 structures the core is passivated with an undoped shell of the same host matrix without the dopant ions, for example $NaYF_4$:Yb^{3+},Er^{3+} (core)/$NaYF_4$ (shell) where the Yb^{3+}, Er^{3+} in the core are the dopant ions responsible for the upconversion luminescence [12]. In type-2 structures selective dopant ions in the shell are also incorporated to generate a doped-core–doped-shell structure. Qian and Zhang demonstrated for the first time the doped-core–doped-shell structure by selectively doping Tm^{3+} in the core and Er^{3+} in the shell ($NaYF_4$:Yb^{3+},Tm^{3+} (core)–$NaYF_4$:Yb^{3+},Er^{3+}(shell)) to generate multicolor upconversion using core–shell structures [13]. A slight variation of this class is the active-core–active-shell structures demonstrated by Capobianco and coworkers [14]. In these structures the shell is doped only with the activator ion (Yb^{3+}) and enhanced upconversion efficiency compared to the undoped shell was demonstrated. The enhancement upconversion with these structures is shown in Fig. 1. As the class-1 core–shell nanocrystals have the same crystalline host

Figure 1 Photographs of colloidal solutions of (a) $NaGdF_4$:Er^{3+},Yb^{3+} active-core–$NaGdF_4$ inert-shell nanoparticles and (b) active-core–active-shell $NaGdF_4$:Er^{3+},Yb^{3+}/$NaGdF_4$:Yb^{3+} nanoparticles in toluene (~1 wt.%) following excitation with 980 nm (note: the two digital photographs were taken using identical camera settings). Reprinted with permission from Ref. [14]. Copyright 2009, Wiley-VCH.

in both the core and the shell, except for the distribution of dopant ions, they can be collectively termed as homo-epitaxial core–shell nanostructures.

In class-2 structures the core and the shell host matrix are of different composition and structures of this type are hetero-epitaxial core–shell nanocrystals. While the class-1 structures allow for luminescence enhancement, class-2 structures can offer both luminescence enhancement and integration of two or more distinct properties. For example, $NaYF_4$:Yb^{3+},Er^{3+} (core)/$NaGdF_4$ (shell) structures have a luminescent upconverting core protected by a $NaGdF_4$ shell, where the paramagnetic Gd^{3+} in the shell allows for integrating magnetic resonance imaging (MRI) properties [15]. Recently, Yan and coworkers demonstrated $NaYF_4$:Yb^{3+},Er^{3+} (core)/CaF_2 (shell) hetero-epitaxial nanocrystals, where the core is cubic (α)-$NaYF_4$ and has similar lattice parameters to CaF_2 in the shell [16]. This work demonstrates that with lattice matching, core–shell structures of completely different chemical compositions can also be constructed. Another unique advantage of the hetero-epitaxial core–shell structures is that it allows for in-depth characterization of the

core–shell morphology, while it still remains a challenge with the homo-epitaxial structures (discussed in section 4). In general, the class-2 hetero-epitaxial structures are still not explored as much as the class-1 homo-epitaxial core–shell structures.

2.3 Advantages and utility of core–shell nanocrystals

The primary advantage and the importance of core–shell structures are the enhancement of the upconversion efficiency of the core nanocrystals as discussed above. The first demonstration of upconversion enhancement in β-$NaYF_4$:Yb^{3+},Er^{3+} (Tm^{3+}) (core)–$NaYF_4$ (shell) nanocrystals was reported by Chow and coworker [12]. They showed that with a ~1.5 nm thick undoped shell of $NaYF_4$ the upconversion emission of a doped 7.7 nm core nanocrystal can be enhanced by 7.4 and 29.6 times for β-$NaYF_4$:Yb^{3+},Er^{3+} and β-$NaYF_4$:Yb^{3+},Tm^{3+} core nanocrystals, respectively. Our group reported the first absolute quantum yield (QY) measurements on the core and core–shell upconverting (β-$NaYF_4$:Yb^{3+},Er^{3+} (core)–$NaYF_4$ (shell)) nanocrystals, and showed a 300% increase in QY (0.10% (core) to 0.30% (core–shell)) after the growth of an undoped $NaYF_4$ shell [10]. Importantly, the core–shell nanocrystals of size 30 nm have the same QY as that of a 100 nm core only nanocrystals, clearly demonstrating the structural advantage of the core–shell morphology.

Depending on the selection of dopant ions unique emission processes can be realized from lanthanide-based nanocrystals. However, co-doping two different emissive ions within a single nanostructure often results in detrimental cross-relaxation and quenching effects that reduce the luminescence from both the doped emissive ions. However, this can be overcome by isolating spatially the different dopant ions in core–shell structures by selectively positioning the emissive ions separately in the core and the shell. As discussed earlier, Qian and Zhang demonstrated for the first time the advantage of core–shell structure in spatial positioning of the dopant ions by selectively doping Tm^{3+} in the core, and Er^{3+} in the shell ($NaYF_4$:Yb^{3+},Tm^{3+} (core)–$NaYF_4$:Yb^{3+},Er^{3+} (shell)) without any deleterious cross-relaxation between the emissive ions [13]. The advantage of this spatial positioning of dopant ions was used to demonstrate "remote-control" photoswitching of dithienylethene (DTE) by Branda and coworkers [17]. They showed that $NaYF_4$ nanocrystals doped with Er^{3+}/Yb^{3+} and Tm^{3+}/Yb^{3+} ions in separate layers change the type of light they emit when the power density of the excitation light (980 nm) is increased/decreased (as the non-linear processes have different power dependencies). At high power densities the dominant ultraviolet (UV) emission triggers the ring-closing of the DTE photoswitches, and when switched to low excitation power the visible light generated triggers the ring-opening reaction to regenerate the original photoisomer (Fig. 2).

The core–shell conformation can also be used for selective energy transfer between the dopant ions in the core and the shell generating unique dual-mode luminescence. In this regard, the first demonstration of Eu^{3+} luminescence both under UV (273 nm) and near-infrared (NIR) excitation (976 nm) was reported in $NaGdF_4$:Yb^{3+},Tm^{3+} (core)/$NaGdF_4$: Eu^{3+} (shell) nanocrystals by Chen and coworkers [18]. The luminescence of the Eu^{3+} ions under UV excitation is sensitized by the Gd^{3+} of the host matrix, while the Yb^{3+} and Tm^{3+}

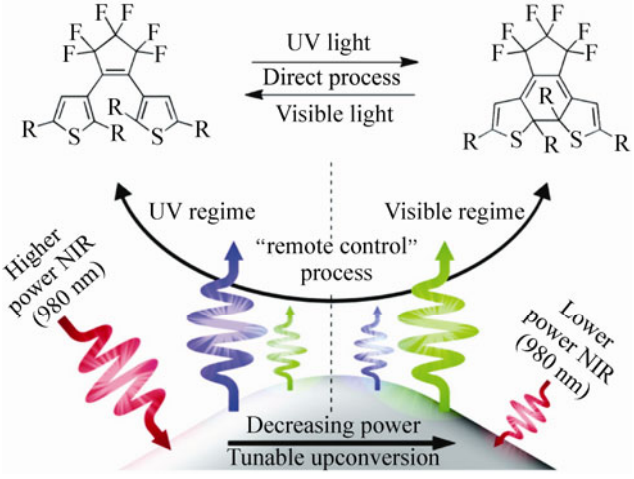

Figure 2 The "direct photoreactions" of the DTE derivatives used in this study are triggered by UV light (for ring-closing) and visible light (for ring-opening). These reactions can also be triggered in a "remote-control" process using the UV light generated under high excitation power densities and the visible light generated under low excitation power densities when the core–shell–shell UCNPs (ErTm and TmEr) absorb near-infrared light (980 nm). The sizes of the colored arrows represent the relative amount of each type of light excited or emitted during the multiphoton process. Reprinted with permission from Ref. [17]. Copyright 2010, American Chemical Society.

in the core act as double sensitizers for the upconverted emission from the Eu^{3+} ions in the shell. This report shows for the first time the interplay of both the host matrix, and the selective dopant ions in the core and the shell allowing for dual-mode luminescence, which can be potentially used for multiplexed luminescent biolabels [19]. Wang et al. extended this interplay of the gadolinium host matrix and the dopant ions (activators) in the shell to a wide range of composition by selectively doping different lanthanide ions in the shell (Tb^{3+}/Dy^{3+}/Sm^{3+}/Eu^{3+}) to generate multicolor upconversion emission by energy migration-mediated upconversion (EMU), demonstrating further the potential utility of core–shell structures [20]. However, the Gd^{3+} lattice in this design is not efficient enough to overcome the surface quenching and this was addressed in a recent report by coating an inert $NaYF_4$ shell [21]. The role of the spatial separation of the Gd^{3+} matrix and the activator ion in the shell was also investigated with a inert $NaYF_4$ interlayer between the core and the doped ion (Tb^{3+}) in the shell as shown in Fig. 3, which highlights the importance of spatial separation and the role of core–shell structures in realizing unique upconversion processes in this class of nanomaterials.

The core–shell structures also offer unique design advantages in integrating different functional applications in a single nanostructure [22, 23]. Reports from Shi and coworkers [15, 24], and also from our group [25], demonstrate that the surface Gd^{3+} ions are the major contributors to the relaxivity enhancement in MRI probes. Moreover, we have demonstrated that the surface Gd^{3+} ions on a larger nanocrystal enhance the T_1 Magnetic resonance imaging (MRI) contrast more strongly than those of smaller nanocrystals, because of the increase in tumbling time with increase in nanocrystal size. Based on this, highly efficient core–shell structures with an upconverting core ($NaYF_4$:Yb^{3+},Tm^{3+}) and a thin shell of $NaGdF_4$ have been realized integrating efficiently both the advantages of upconversion and magnetic resonance imaging in a single nanostructure [26].

The utility of the core–shell structural composition is thus not limited to luminescence enhancement alone, and can potentially be used to generate multifunctional colloidal nanostructures with specific

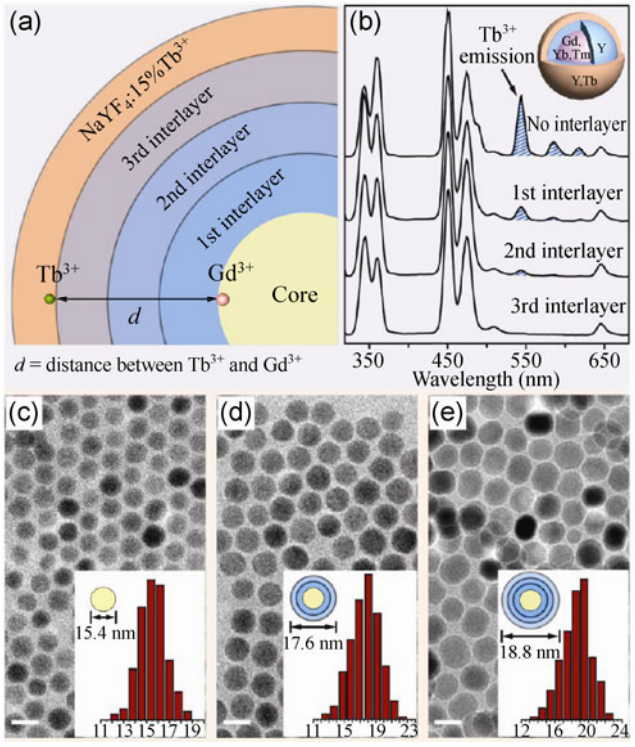

Figure 3 (a) Schematic design for controlling energy transfer from Gd^{3+} to Tb^{3+} through layer-by-layer growth technique. (b) Emission spectra of the $NaGdF_4$:Yb^{3+},Tm^{3+}/$NaYF_4$/$NaYF_4$:Tb^{3+} (core–shell–shell) nanoparticles with different thickness of $NaYF_4$ interlayer. (c)–(e) Corresponding TEM images of the as-prepared nanoparticles (insets are histograms of the particle size distribution). Note that each interlayer was prepared using a 5 mL of $NaYF_4$ precursor. Reprinted with permission from Ref. [21]. Copyright 2012, American Chemical Society.

functional applications [27, 28]. The necessity of generating such compositional versatility in core–shell nanocrystals while maintaining their high-quality needs an in-depth understanding of the growth mechanism [29], allowing further advancement in realizing the potential applications of core–shell structures.

3 Synthesis and epitaxial growth mechanism of core–shell nanocrystals

3.1 Synthesis techniques of core–shell nanocrystals

The classification of epitaxial shell growth techniques on core β-$NaYF_4$ nanocrystals is generally based on the method of incorporating the shell precursors to grow the shell. Based on this, the conventional core–shell synthesis approaches can be classified as shell growth

by the hot-injection method, and shell growth by the heat-up method. In the hot-injection method shell precursors dissolved in high boiling solvents are injected directly into the hot reaction mixture after the core nanocrystals have formed to grow the shell. In the heat-up method the core nanocrystals are pre-synthesized and then mixed with the shell precursors and high boiling solvents separately and subsequently heated to higher temperatures to grow the shell.

The first report of shell growth on β-$NaYF_4$:Yb^{3+},Er^{3+} nanocrystals was based on the hot-injection method [12]. Using sodium trifluoroacetate (CF_3COONa) and yttrium trifluoroacetate ($(CF_3COO)_3Y$) mixed in oleylamine as shell precursors followed by slow addition to the core (β-$NaYF_4$:Yb^{3+},Er^{3+}) reaction mixture Yi and Chow demonstrated the growth of an undoped $NaYF_4$ shell on the core nanocrystals as shown in Fig. 4. Capobianco and coworkers extended this strategy to $NaGdF_4$ nanocrystals and demonstrated β-$NaGdF_4$:Er^{3+},Yb^{3+}/$NaGdF_4$:Yb^{3+} active-core–active-shell

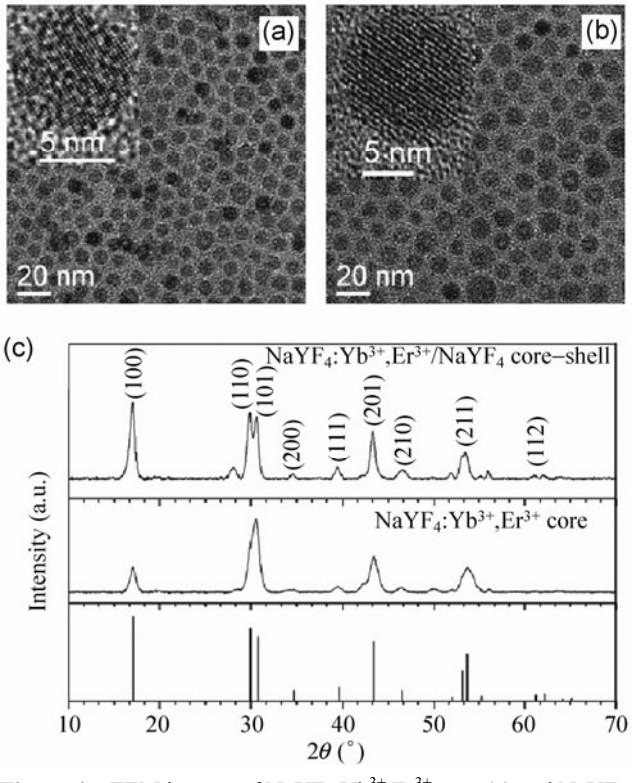

Figure 4 TEM images of $NaYF_4$:Yb^{3+},Er^{3+} core (a) and $NaYF_4$:Yb^{3+},Er^{3+}/$NaYF_4$ core–shell (b) and XRD patterns of these nanocrystals (c). The bottom part of (c) is the line pattern of β-$NaYF_4$ (PDF 28-1192). Reprinted with permission from Ref. [12]. Copyright 2007, American Chemical Society.

nanocrystals [14]. Recently, Zhao and coworkers demonstrated hetero-epitaxial core–shell structures by successive injection of the shell precursors to generate tunable shells of $NaYF_4$ on β-$NaGdF_4$:Er^{3+},Yb^{3+} nanocrystals [30]. Deviating from the general hot-injection approach, they used a two-step approach, wherein pre-synthesized core nanocrystals were used and mixed with the high-boiling solvents separately and the shell precursors were later introduced into the reaction mixture at higher temperature.

In spite of the successful demonstration of up-conversion enhancement after shell growth with the hot-injection method, the majority of core–shell structures synthesized to date are based on the heat-up method. The necessity of slow and controlled injection of the molecular shell precursors to avoid homogenous nucleation of the precursors remains a major hurdle with this synthetic approach.

The widely used synthesis protocol based on heat-up method for the β-$NaYF_4$ core–shell nanocrystals was developed by Qian and Zhang [13]. The ability to make uniform core–shell nanocrystals rely on the uniformity of the core nanocrystals, and their group was the first to demonstrate a simple and user-friendly reproducible synthesis of β-$NaYF_4$:Er^{3+},Yb^{3+} core nanocrystals [31]. They developed the heat-up method for shell growth following the same procedure as the core nanocrystal synthesis. For the shell growth, the shell precursors are homogenously mixed with the organic solvents similar to the core synthesis and subsequently the pre-synthesized uniform core nanocrystals are added and heated to higher temperature following the core synthesis procedure. They demonstrated a doped-core–doped-shell structure with Yb^{3+},Tm^{3+} ions in the core, and Yb^{3+},Er^{3+} ions in the shell as shown in Fig. 5. They extended the structural morphology further by synthesizing a core–shell–shell type nanocrystal for the first time by adding another doped-shell of $NaYF_4$ with Yb^{3+},Tm^{3+} ions to the above core–shell structure [13]. The successful synthesis of multi-layer shell growth and spatial positioning of dopant ions within the shell for the first time demonstrated the synthetic advantage of the heat-up method to generate core–shell structures of unique structural compositions.

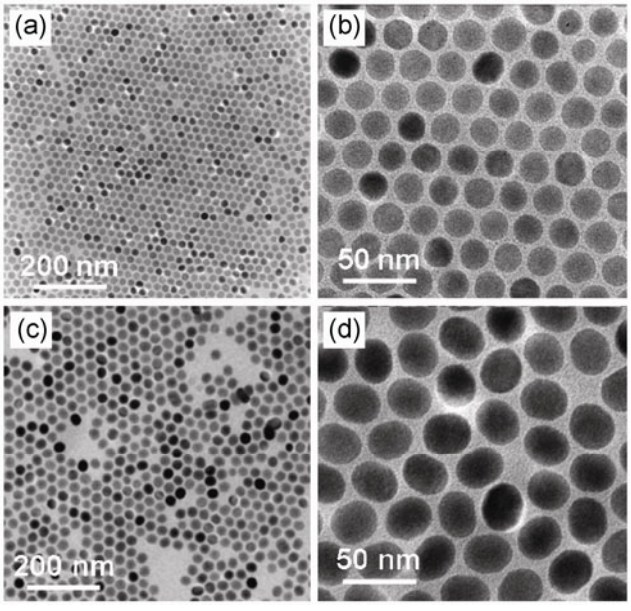

Figure 5 TEM images of monodisperse $NaYF_4$:Yb^{3+},Tm^{3+} nanocrystals (a), (b) and core–shell $NaYF_4$:Yb^{3+},Tm^{3+}@$NaYF_4$:Yb^{3+},Er^{3+} nanocrystals (c), (d). Reprinted with permission from Ref. [13]. Copyright 2008, American Chemical Society.

The heat-up method is generally referred to as seed-mediated shell growth, where the pre-synthesized core nanocrystals are expected to act as nuclei/seeds for the shell growth. At least in this class of nanocrystals this is not true (as will be discussed in the following section under growth mechanism), and to highlight this difference, this synthesis methodology is simply referred to as the heat-up method.

Although the heat-up method is widely used, some important synthesis parameters need to be considered when core–shell structures of different shell thickness and compositions are explored. The reaction time for the synthesis of the core, core–shell, and core–shell–shell structures of the same host matrix composition is not the same [32]. The shell growth time increases with size and needs a trial-and-error approach to get a unimodal distribution of core–shell nanostructures. Liu and coworkers have established that the shell growth is affected by the shell precursor concentration and also the size of the core nanocrystals used [20]. These aspects need to be considered when core–shell structures of different structural composition are synthesized by this approach.

To overcome some of the limitations in the above discussed conventional shell growth techniques, we reported a shell growth technique based on nanocrystal size dependent dissolution and growth driven by Ostwald ripening [33]. We showed that small sacrificial nanocrystals (SNCs) as shell precursors directly injected into the core reaction mixture (without any control over the injection rate) rapidly dissolve and deposit onto the larger core nanocrystals (through self-focusing) to generate core–shell structured nanocrystals (Fig. 6). This protocol takes advantage of the common physical phenomenon of ripening in colloids, where larger particles (i.e., core nanocrystals) grow at the expense of energetically less stable smaller particles (i.e., SNCs). In this approach, the shell thickness can be tuned either by manipulating the number of SNCs injected or the SNCs can be injected successively into the core reaction mixture to generate layer-by-layer epitaxial growth. Depending on the injected SNCs core–shell structures of various homo- and hetero-structure compositions can be generated using this approach. Haase and coworkers have also utilized this protocol to synthesize tunable $NaGdF_4$ shells on $NaYF_4$ core nanocrystals [34]. However, the

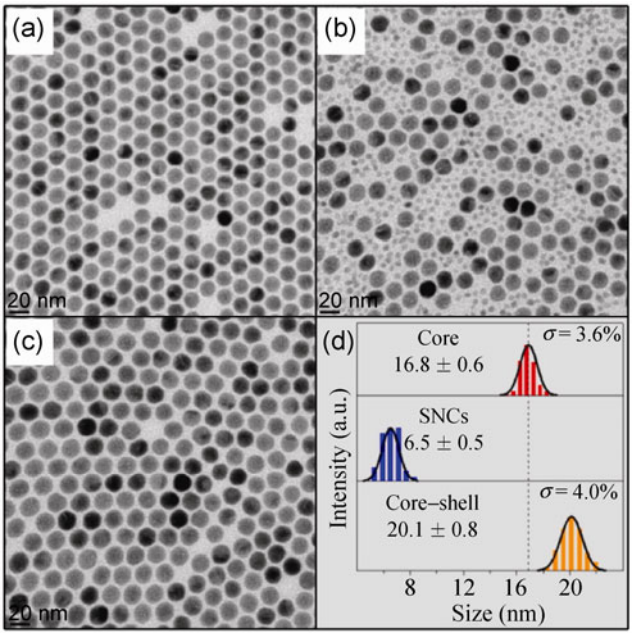

Figure 6 (a)–(c) TEM of $NaYF_4$:Yb^{3+},Er^{3+} core nanocrystals, after injection of sacrificial $NaYF_4$ nanocrystals, and after self-focusing $NaYF_4$:Yb^{3+},Er^{3+} core–$NaYF_4$ shell nanocrystals, respectively, and (d) size distribution of the nanocrystals. Reprinted with permission from Ref. [33]. Copyright 2012, American Chemical Society.

extension of this protocol to smaller core nanocrystals (~5 nm) is challenging as the SNCs need to be smaller than the core NCs.

3.2 Core–shell growth mechanism

The growth mechanism of core–shell structures within this class of nanocrystals remains largely unexplored and is generally presumed to be identical to other material systems. The nucleation and growth mechanism of the β-$NaLnF_4$ core nanocrystals is known to vary along the lanthanide series depending on the lanthanide host matrix, as previously shown by Yan and coworkers [35]. This variation in the nucleation/growth depending on the lanthanide host should indeed play a role in the growth of core–shell structures, and thus cannot be presumed to be identical to other material systems or even within different lanthanide shell matrix compositions. Moreover, given that a wide range of core–shell structural composition (section 2.2) can be realized in this class of nanostructures it is also not possible to propose a common/general shell growth mechanism. In this section, we will discuss the shell growth mechanism in the widely used upconverting β-$NaYF_4$:Yb^{3+},Er^{3+}/$NaYF_4$ core–shell structures, and highlight why the growth mechanism cannot be presumed to be identical to other material systems.

The widely used heat-up method to synthesize core–shell upconverting (β-$NaYF_4$:Yb^{3+},Er^{3+}/$NaYF_4$) nanocrystals with an undoped shell is generally referred as seed-mediated shell growth. Based on conventional shell growth mechanism, the core nanocrystals are believed to act as seeds/nuclei for the epitaxial deposition of the shell material generating core–shell structures. This general assumption for epitaxial deposition of the shell on the core nanocrystals is often supported by two general arguments, (i) the lower surface tension and low energy barrier that needs to be overcome on a pre-existing particle (core–seed particles), as opposed to forming a new particle (from the shell precursors), favors the deposition of the shell precursors on the surface of the core nanocrystals [36], and (ii) the core–shell nanocrystals are larger than the seed (core) nanocrystals, and the absence of small nanocrystals in the core–shell ensemble (at the end of the reaction) suggests that the core nanocrystals indeed acted as seed nanocrystals for epitaxial shell growth [13].

However, in our recent report we showed that these assumptions are not correct for epitaxial shell growth mechanism in this class of nanostructures [33]. During the course of the core–shell reaction we retrieved multiple aliquots of reaction mixture at different reaction time/temperature and analyzed the reaction product by TEM and XRD (Fig. 7). The formation of the shell material as separately nucleated kinetic phase (α-$NaYF_4$) product dominates at the early stages of the shell growth reaction. The broad

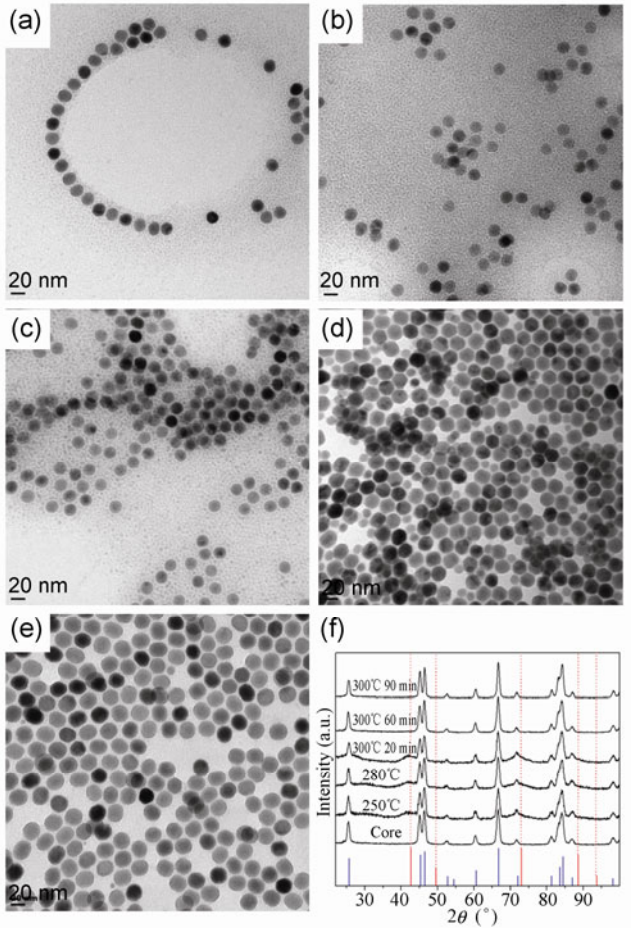

Figure 7 TEM images of core–shell nanocrystals at different reaction time/temperature (a) 250 ˚C; (b) 280 ˚C; (c) 300 ˚C for 20 min; (d) 300 ˚C for 60 min; (e) 300 ˚C for 90 min; and (f) XRD spectra of the core and the core–shell nanocrystals at different reaction time/temperature, and the standard reference patterns of α-$NaYF_4$ (red), and β-$NaYF_4$ (blue) (JCPDS: 06-0342-α-$NaYF_4$, 016-0334-β-$NaYF_4$).

feature in the XRD patterns at 42° and 73° (2θ) confirms the presence of small kinetic phase $NaYF_4$ at the early stage of the reaction. Only at elevated temperature (300 °C) and after prolonged heating the shell material nucleated as small α-$NaYF_4$ dissolves and deposits on the larger core β-$NaYF_4$:Yb^{3+},Er^{3+} nanocrystals generating the core–shell (β-$NaYF_4$:Yb^{3+},Er^{3+}/$NaYF_4$) structures. This deviation in the core–shell growth mechanism arises from the low energy barrier for the nucleation of the kinetic phase (α-$NaYF_4$) [35] compared to the direct growth of the shell precursors as thermodynamic phase (β-$NaYF_4$) shell on pre-existing core (β-$NaYF_4$:Yb^{3+},Er^{3+}) nanocrystals (seeds). The general growth mechanism in heat-up shell growth is the separate nucleation and formation of the shell precursors as kinetic phase α-$NaYF_4$ nanocrystals at lower temperature followed by ripening-mediated deposition of these separately nucleated shell nanocrystals on the larger thermodynamically stable core β-$NaYF_4$:Yb^{3+},Er^{3+} nanocrystals to form β-$NaYF_4$:Yb^{3+},Er^{3+}/$NaYF_4$ core–shell structures.

The core–shell growth mechanism in other heat-up based systems, such as β-$NaGdF_4$:Yb^{3+},Er^{3+}/$NaGdF_4$, or β-$NaYF_4$:Yb^{3+},Er^{3+}/$NaGdF_4$ where a shell matrix of $NaGdF_4$ is grown may not necessarily be the same as that discussed for β-$NaYF_4$:Yb^{3+},Er^{3+}/$NaYF_4$ core–shell structures. In case of β-$NaGdF_4$ the ionic radius of Gd^{3+} matches well with the Na^+ and even under milder reaction conditions the gadolinium precursors can nucleate directly as β-$NaGdF_4$ without forming the kinetic phase α-$NaGdF_4$ [35]. Even in these core–shell systems, where the hexagonal phase (β-$NaGdF_4$) is favored, it does not necessarily result in direct deposition of the shell material on the core–seed hexagonal phase nanocrystals, as recently observed by Liu and coworkers [20]. Our group has also reported on the presence of small amounts of separately nucleated β-$NaGdF_4$ nanocrystals during the growth of β-$NaYF_4$/$NaGdF_4$ core–shell nanocrystals [37]. This emphasizes the fact that even in systems where the hexagonal phase is preferred, the separate nucleation of the shell precursors could happen under the reaction conditions widely employed in the heat-up shell growth reaction.

The understanding of core–shell growth mechanism along the lanthanide series is still limited, and the highlighted examples in this section demonstrates the need for additional systematic evaluations to advance our understanding of the shell growth mechanism in this class of nanostructures. As discussed here, the conventional shell growth mechanism is not directly applicable to these systems and further studies need to be performed to have a generalized understanding of the shell growth process.

4 Characterization of core–shell nanocrystals

4.1 Indirect evidence for core–shell structures

In general, the confirmation of shell growth is based on TEM analysis showing crystallite size increases of the core–shell structures compared to the core nanocrystals, accompanied by narrowing of the XRD peaks as the crystallite size increases [12]. Especially in case of homo-epitaxial core–shell structures, where the shell and the core have the same matrix composition except for the positioning of dopant ions, allows only for such indirect evidence of shell growth based solely on crystallite size increase. The luminescence enhancement with shell growth provides further confirmation for core–shell structures as the shell shields the core from surface and solvent quenching [33]. The nanocrystal size increase and luminescence enhancement after shell growth taken together provide evidence for core–shell homo-epitaxial structures (Fig. 8).

The primary limitation in using the nanocrystal size increase/luminescence enhancement as a proof for core–shell structure is that it does not provide structural details of the shell layer relative to the core. Such indirect evidence does not necessarily confirm the presence of a uniform shell around the core nanocrystals (ideal core–shell), but is consistent with it. The shape evolution of the core–shell nanocrystals relative to the core should also be taken into account when homo-epitaxial core–shell nanocrystals are characterized (discussed in section 5), and is a first indication of the morphology of shell growth. In this regard, interpreting the core–shell structures using such indirect evidence should be made with great caution. To date, for the homo-epitaxial core–shell nanocrystals the structural characterization remains limited to such indirect evidence.

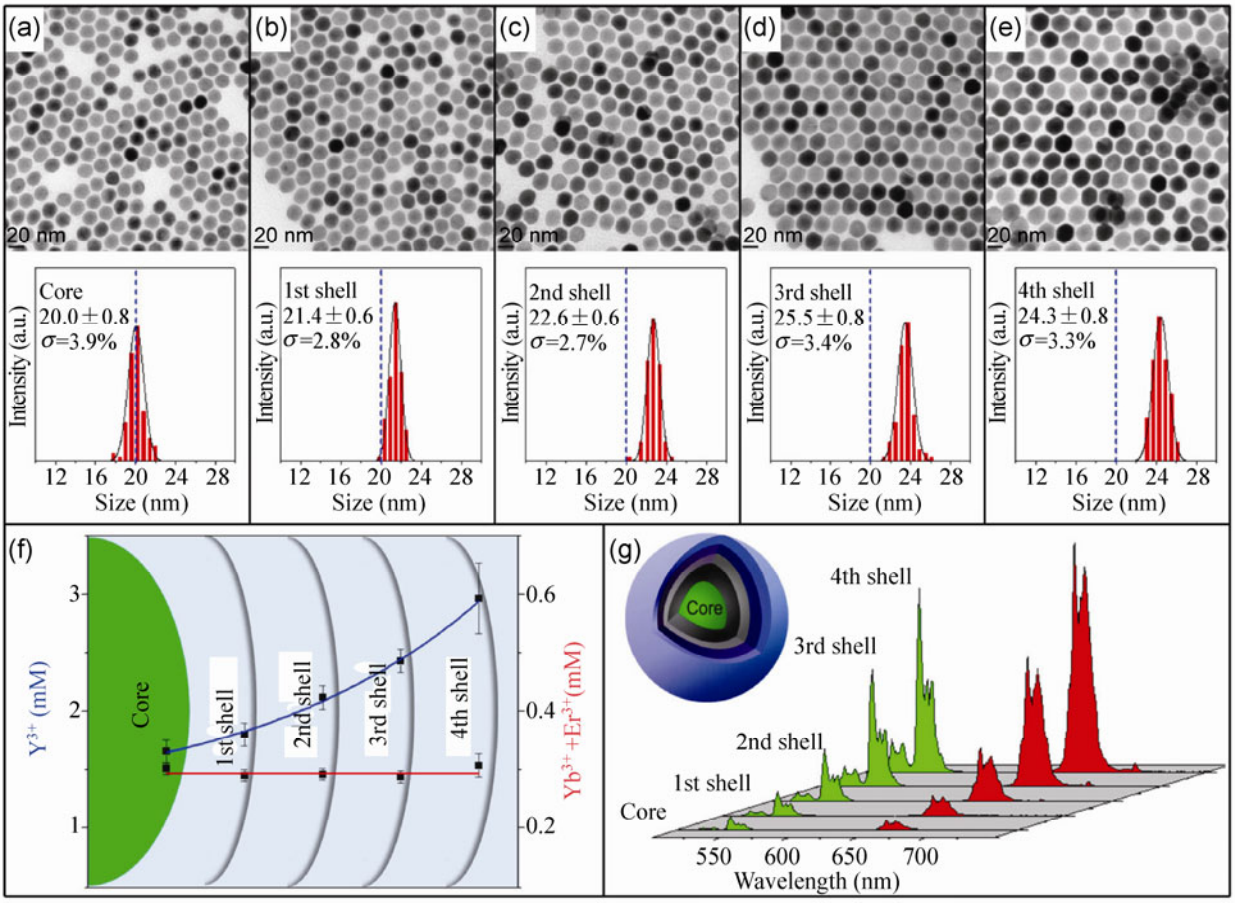

Figure 8 (a)–(e) TEM images and size distribution of $NaYF_4$:Yb^{3+}/Er^{3+} (15%/2%) core NCs (@t=0), $NaYF_4$:Yb^{3+},Er^{3+} (15%/2%) core–$NaYF_4$ shell NCs after successive layer-by-layer epitaxial growth @ t = 5, 10, 15, and 20 min, respectively. (f) ICP-MS elemental analysis of the core and core–shell NCs with same number concentration of NCs. (g) Upconversion emission spectra of the hexane dispersions of core and core–shell NCs with same number concentration of NCs under 980 nm excitation. Reprinted with permission from Ref. [33]. Copyright 2012, American Chemical Society.

4.2 Direct evidence for core–shell structures

In case of hetero-epitaxial core–shell structures where the core and shell matrix are not the same it is possible to study the structural morphology of the core–shell nanocrystals using various characterization techniques. Our group reported the first direct evidence for core–shell structures in these classes of nanocrystals using X-ray photoelectron spectroscopy (XPS) based on tunable synchrotron radiation [38]. Using $NaYF_4$/$NaGdF_4$ core–shell nanocrystals, the intensity ratios of the Y^{3+} 3d to Gd^{3+} 4d core levels were studied in different kinetic energy ranges. The Y^{3+}/Gd^{3+} ratio increases with increasing kinetic energy, showing that the Gd^{3+} from the shell screens the Y^{3+} intensity from the core thus providing direct evidence for a core–shell structure. While this characterization technique does provide a confirmation of core–shell structure, it is an ensemble measurement and does not provide any structural details about individual nanocrystals and the shell morphology/thickness of the final core–shell structures.

Direct evidence for core–shell structures (either on an ensemble or individual nanocrystal) can be obtained using scanning transmission electron microscopy (STEM) combined with techniques such as high-angle annular dark-field (HAADF) imaging, electron energy loss spectroscopy (EELS), and energy-dispersive X-ray spectroscopy (EDS). We have reported on the advantages of these individual techniques in characterizing

core–shell structures [37]. HAADF imaging takes advantage of the difference in atomic number of the core and shell matrix, and the contrast scales, to a first approximation, proportionally to the square of the atomic number. For example, *Z*-contrast HAADF images of $NaYF_4$/$NaGdF_4$ core–shell nanocrystals show a clear contrast between the core which appears dark (yttrium $Z = 39$,) while the shell appears bright (gadolinium $Z = 64$). This technique was also used to confirm $NaYF_4$/CaF_2 core–shell structures (Fig. 9), and in this case the contrast is reversed where the core (yttrium-rich) appears bright compared to the shell (calcium-rich) [16, 39]. The ability to confirm the core–shell structural morphology on an ensemble makes this technique attractive. However, this technique is limited as it is only useful when there is a large enough difference in atomic number between the core and the shell matrix composition. A complicating factor in the analysis could be that strain also adds to the contrast, depending on the orientation of the particles with respect to the electron beam [40].

EELS and EDS allow for obtaining chemical composition of individual nanocrystals by scanning the beam across the particle [37]. The line scans performed on individual nanocrystals allows for confirming of both the chemical composition and the shell distribution around the nanocrystal (Fig. 10). We have also employed EELS 2D elemental mapping of the whole nanoparticle to analyze the core–shell morphology [26, 33]. However, the long acquisition times for the line scans and elemental mapping result in considerable beam damage of the nanocrystal before useful information on the core–shell composition could be obtained. Therefore, we always collect a bright-field image of the mapped area to check on the integrity of the sample. Recently, Zhao and coworkers demonstrated the use of cryo-TEM operating at 96 K to minimize the electron beam damage and provided confirmation of core–shell structures at the sub-nanometer level [41].

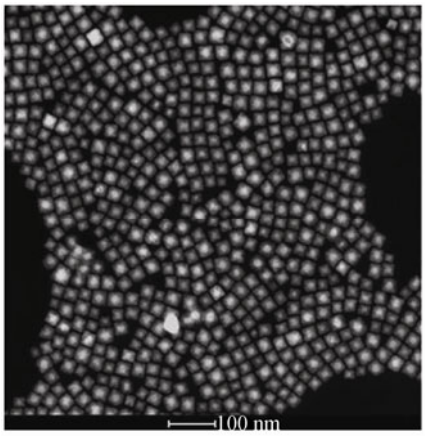

Figure 9 High-angle annular dark-field scanning transmission electron microscopy image of $NaYbF_4$:Tm^{3+}/CaF_2 core–shell structures; both the core (bright) and the shell (dark) are clearly visible. Reprinted with permission from Ref. [39]. Copyright 2012, American Chemical Society.

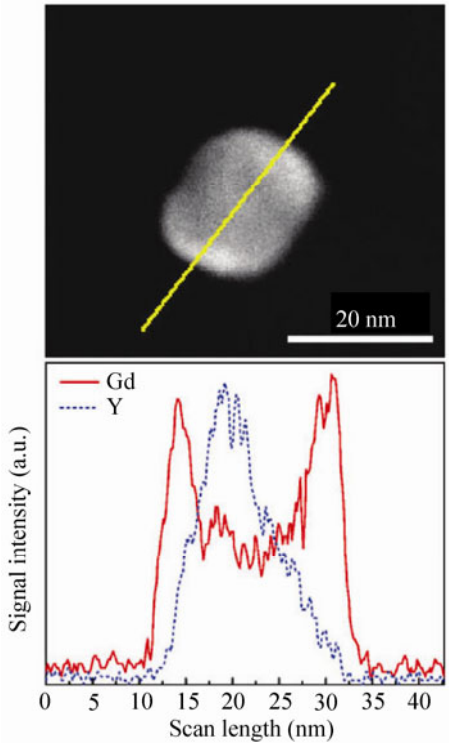

Figure 10 EDS line scan across a single $NaYF_4$/$NaGdF_4$ core–shell NC showing Y in the core of the particle and Gd located in the shell. Reprinted with permission from Ref. [37]. Copyright 2011, American Chemical Society.

The multiple characterization techniques discussed here, when collectively used, give a much better insight on the formation of core–shell structure and their chemical composition. However, these techniques are limited to the hetero-epitaxial structures and necessitate sample stability under the electron beam [37]. The later should be taken into account when structural morphology is determined and results should be interpreted with caution.

5 Remarks on core–shell structural morphology

The chemical similarity of the lanthanides and the minimal variations in the lattice constants within these structures are often expected to allow for isotropic/centrosymmetric epitaxial growth in this class of nanostructures. The first evidence of core–shell growth in lanthanide-based nanocrystals reported by Haase and coworkers showed that the $CePO_4/LaPO_4$ core–shell structures are rather anisotropic in shape [4]. In case of $NaLnF_4$ structures the shell growth in spite of the observed anisotropic shape after epitaxial growth is often overlooked and generally interpreted as isotropic structures [42]. In this section we focus on the structural morphology of the core–shell (homo/hetero-epitaxial) structures of $NaLnF_4$ developed to date, and compare it with the structural motif of core–shell (centrosymmetric and non-centrosymmetric shell growth) structures discussed in section 2.1.

5.1 Structural morphology of hetero-epitaxial core–shell nanocrystals

The hetero-epitaxial structures, as explained earlier, allow for better insight into the core–shell structure and chemical composition. In $NaYF_4/NaGdF_4$ core–shell structures, EELS line scans on multiple core–shell nanocrystals revealed that the $NaGdF_4$ shell growth is anisotropic and not centrosymmetric relative to the core $NaYF_4$ (Fig. 11). Line scans performed in one direction can show a symmetrical shell distribution (Fig. 10), but this is not necessarily the case if performed in another direction and the shell thickness/distribution varies (Fig. 11) in each individual structure. For the first time, this work highlighted the structurally anisotropic shell growth in this class of nanocrystals [37].

The anisotropic shell growth of $NaGdF_4$ on $NaYF_4$ core nanocrystals in spite of the minimal lattice mismatch of ~2% remains unexplained. The above evidence of anisotropic shell growth on these structures can also be observed in core–shell structures of $NaYF_4/NaGdF_4$ reported by other research groups [15, 43]. The anisotropic growth of $NaGdF_4$ on doped $NaYF_4$ core structures as seen in their shape deformation after shell growth is shown in Fig. 12. For thin shell growth the core–shell structures do remain

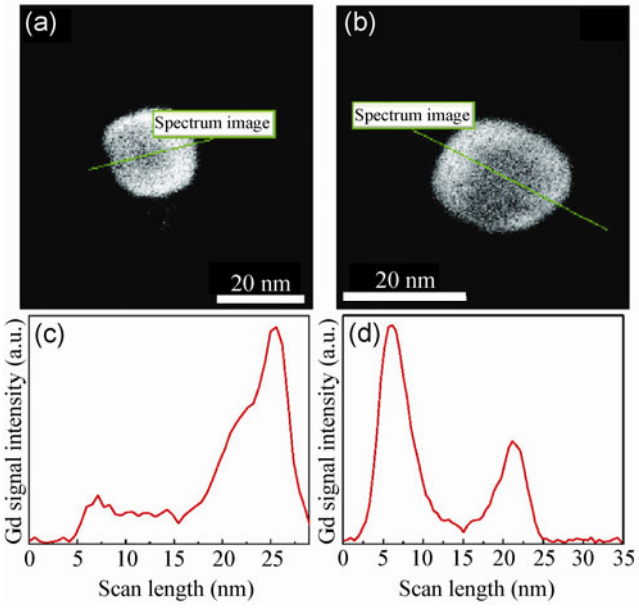

Figure 11 (a) and (b) HAADF images of single $NaYF_4/NaGdF_4$ core–shell NCs and the corresponding (c) and (d) EELS line scans showing non-uniform shell distribution. Reprinted with permission from Ref. [37]. Copyright 2011, American Chemical Society.

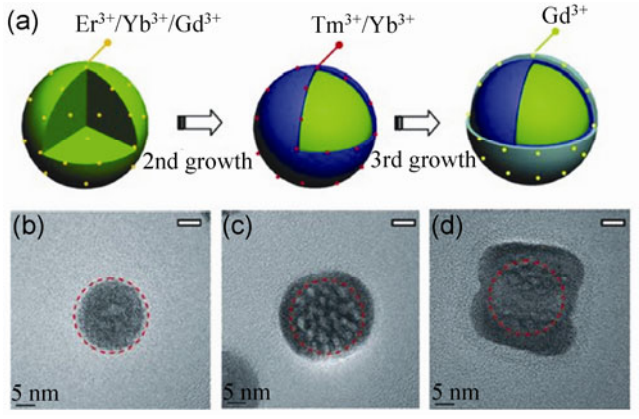

Figure 12 (a) Schematic illustration of core–multi-shell NCs, $NaYF_4:Er^{3+}/Yb^{3+}/Gd^{3+}$ core, $NaYF_4:Tm^{3+}/Yb^{3+}$ first shell, and $NaGd_4$ second shell, and (b)–(d) respective HRTEM images of the core, core–shell, core–shell–shell NCs. Reprinted with permission from Ref. [15]. Copyright 2011, Wiley-VCH.

isotropic in shape [15, 33], and with increased shell thickness (>2 nm) the shell growth is generally anisotropic for these structures.

5.2 Structural morphology of homo-epitaxial core–shell nanocrystals

Direct evidence for shell distribution on the core nanocrystals is hard to obtain in case of homo-

epitaxial core–shell structures. However, the shape evolution of the core–shell nanocrystals compared to the starting core nanocrystals does provide insights into the structural morphology. Upconverting β-$NaYF_4$:Yb^{3+},Er^{3+} core nanocrystals which are quasi-spherical in shape after $NaYF_4$ shell growth transform into oblong core–shell structures (Figs. 5 and 13). Especially,

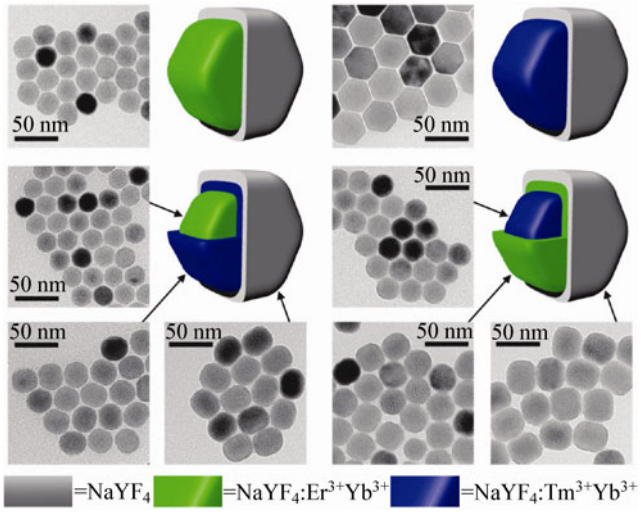

Figure 13 TEM images of the core, core–shell, core–shell–shell nanoparticles for $NaYF_4$:Er^{3+},Yb^{3+}/$NaYF_4$, $NaYF_4$:Tm^{3+},Yb^{3+}/$NaYF_4$, $NaYF_4$:Er^{3+},Yb^{3+}/$NaYF_4$:Tm^{3+},Yb^{3+}/$NaYF_4$, and $NaYF_4$:Tm^{3+},Yb^{3+}/$NaYF_4$:Er^{3+},Yb^{3+}/$NaYF_4$. Reprinted with permission from Ref. [17]. Copyright 2010, American Chemical Society.

when thick shells (>2–3 nm) are grown, the structural anisotropy based on shape evolution is identical to that discussed for hetero-epitaxial core–shell structures. Almost all core–shell and core–shell–shell structures developed to date do not confine to the centrosymmetric (ideal) core–shell model shown as defined in Scheme 1(a). Based on structural morphology these structures resemble the non-centrosymmetric core–shell model (Scheme 1(b)), and the shell growth is anisotropic.

Recently, Zhao and coworkers reported β-$NaGdF_4$:Yb^{3+},Er^{3+}/$NaYF_4$ core–shell structures which are highly uniform and isotropic in shape [30]. Using ~4.5 nm core (β-$NaGdF_4$:Yb^{3+},Er^{3+}) nanocrystals, they showed that the core–shell structures remain uniform even after 20 monolayer thickness of $NaYF_4$ shell growth (Fig. 14). The core–shell structures in this work conform to the centrosymmetric model shown in Scheme 1(a), and to our knowledge, this is the only work that has shown centrosymmetric shell growth and direct evidence for it using HAADF imaging. However, it still remains to be seen if such isotropic structures are possible on larger core nanocrystals, and other core–shell compositions discussed earlier. Understanding the parameters that govern the isotropic shell growth is still limited, and we emphasize that confirmation of

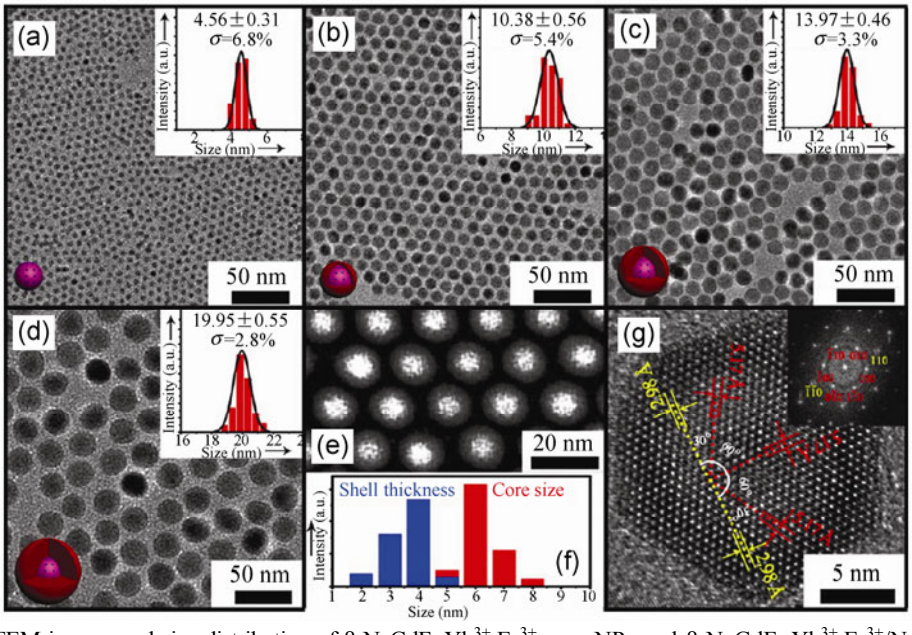

Figure 14 (a)–(d) TEM images and size distribution of β-$NaGdF_4$:Yb^{3+},Er^{3+} core NPs and β-$NaGdF_4$:Yb^{3+},Er^{3+}/$NaYF_4$ core–shell NPs with different shell thickness. (e)–(g) HAADF-STEM, core size and shell thickness distributions, HRTEM image of the core–shell NPs. Reprinted with permission from Ref. [30]. Copyright 2013, American Chemical Society.

shell growth should take into account the structural morphology/shape evolution of the core–shell structures and not just the overall (averaged) size increase.

5 Conclusions

In summary, rational design of core–shell structures of $NaLnF_4$ nanocrystals has shown significant progress both in synthesis and demonstration of their potential applications. However, understanding of the shell growth mechanism is still limited and this will be critical in designing more complex core–shell structures. The core–shell structures in general are not centrosymmetric (ideal) and this problem remains to be addressed. In addition, the underlying growth parameters that lead to anisotropic non-centrosymmetric shell growth over the desired isotropic centrosymmetric shell growth need to be studied and understood in depth. Such progress will require detailed structural characterization of the core–shell composition and morphology. To advance and exploit the unique structural properties of the core–shell $NaLnF_4$ nanostructures designing ideal centrosymmetric core–shell structures will be essential, and should remain the focus in future studies.

References

[1] Chaudhuri, R. G.; Paria, S. Core/shell nanoparticles: Classes, properties, synthesis mechanisms, characterization, and applications. *Chem. Rev.* **2012**, *112*, 2373–2433.

[2] Cozzoli, P. D.; Pellegrino, T.; Manna, L. Synthesis, properties and perspectives of hybrid nanocrystal structures. *Chem. Soc. Rev.* **2006**, *35*, 1195–1208.

[3] Reiss, P.; Protière, M.; Li, L. Core/shell semiconductor nanocrystals. *Small* **2009**, *5*, 154–168.

[4] Kömpe, K.; Borchert, H.; Storz, J.; Lobo, A.; Adam, S.; Möller, T.; Haase, M. Green-emitting $CePO_4$:Tb/$LaPO_4$ core–shell nanoparticles with 70% photoluminescence quantum yield. *Angew. Chem. Int. Edit.* **2003**, *42*, 5513–5516.

[5] Stouwdam, J. W.; van Veggel, F. C. J. M. Improvement in the luminescence properties and processability of LaF_3/Ln and $LaPO_4$/Ln nanoparticles by surface modification. *Langmuir* **2004**, *20*, 11763–11771.

[6] Haase, M.; Schäfer, H. Upconverting nanoparticles. *Angew. Chem. Int. Edit.* **2011**, *50*, 5808–5829.

[7] Auzel, F. Upconversion and anti-Stokes processes with f and d ions in solids. *Chem. Rev.* **2004**, *104*, 139–173.

[8] Menyuk, N.; Pierce, J. W.; Dwight, K. $NaYF_4$-Yb,Er—Efficient upconversion phosphor. *Appl. Phys. Lett.* **1972**, *21*, 159–161.

[9] Krämer, K. W.; Biner, D.; Frei, G.; Güdel, H. U.; Hehlen, M. P.; Lüthi, S. R. Hexagonal sodium yttrium fluoride based green and blue emitting upconversion phosphors. *Chem. Mater.* **2004**, *16*, 1244–1251.

[10] Boyer, J. C.; van Veggel, F. C. J. M. Absolute quantum yield measurements of colloidal $NaYF_4$:Er^{3+},Yb^{3+} upconverting nanoparticles. *Nanoscale* **2010**, *2*, 1417–1419.

[11] Carbone, L.; Cozzoli, P. D. Colloidal heterostructured nanocrystals: Synthesis and growth mechanisms. *Nano Today* **2010**, *5*, 449–493.

[12] Yi, G. S.; Chow, G. M. Water-soluble $NaYF_4$:Yb,Er(Tm)/$NaYF_4$/polymer core/shell/shell nanoparticles with significant enhancement of upconversion fluorescence. *Chem. Mater.* **2007**, *19*, 341–343.

[13] Qian, H. S.; Zhang, Y. Synthesis of hexagonal-phase core–shell $NaYF_4$ nanocrystals with tunable upconversion fluorescence. *Langmuir* **2008**, *24*, 12123–12125.

[14] Vetrone, F.; Naccache, R.; Mahalingam, V.; Morgan, C. G.; Capobianco, J. A. The active-core/active-shell approach: A strategy to enhance the upconversion luminescence in lanthanide-doped nanoparticles. *Adv. Funct. Mater.* **2009**, *19*, 2924–2929.

[15] Chen, F.; Bu, W.; Zhang, S.; Liu, X.; Liu, J.; Xing, H.; Xiao, Q.; Zhou, L.; Peng, W.; Wang, L.; Shi, J. Positive and negative lattice shielding effects co-existing in Gd(Ⅲ) ion doped bifunctional upconversion nanoprobes. *Adv. Funct. Mater.* **2011**, *21*, 4285–4294.

[16] Wang, Y. F.; Sun, L. D.; Xiao, J. W.; Feng, W.; Zhou, J. C.; Shen, J.; Yan, C. H. Rare-earth nanoparticles with enhanced upconversion emission and suppressed rare-earth-ion leakage. *Chem. Eur. J.* **2012**, *18*, 5558–5564.

[17] Boyer, J. C.; Carling, C. J.; Gates, B. D.; Branda, N. R. Two-way photoswitchingusing one type of near-infrared light, upconverting nanoparticles, and changing only the light intensity. *J. Am. Chem. Soc.* **2010**, *132*, 15766–15772.

[18] Liu, Y. S.; Tu, D. T.; Zhu, H. M.; Li, R. F.; Luo, W. Q.; Chen, X. Y. A strategy to achieve efficient dual-mode luminescence of Eu^{3+} in lanthanides doped multifunctional $NaGdF_4$ nanocrystals. *Adv. Mater.* **2010**, *22*, 3266–3271.

[19] Liu, Y.; Tu, D.; Zhu, H.; Ma, E.; Chen, X. Lanthanide-doped luminescent nano-bioprobes: From fundamentals to biodetection. *Nanoscale* **2013**, *5*, 1369–1384.

[20] Wang, F.; Deng, R.; Wang, J.; Wang, Q.; Han, Y.; Zhu, H.; Chen, X.; Liu, X. Tuning upconversion through energy migration in core–shell nanoparticles. *Nat. Mater.* **2011**, *10*, 968–973.

[21] Su, Q.; Han, S.; Xie, X.; Zhu, H.; Chen, H.; Chen, C.-K.; Liu, R.-S.; Chen, X.; Wang, F.; Liu, X. The effect of surface coating on energy migration-mediated upconversion. *J. Am. Chem. Soc.* **2012**, *134*, 20849–20857.

[22] Tu, D.; Liu, Y.; Zhu, H.; Chen, X. Optical/magnetic multimodal bioprobes based on lanthanide-doped inorganic nanocrystals. *Chem. Eur. J.* **2013**, *19*, 5516–5527.

[23] Kar, A.; Patra, A. Impacts of core–shell structures on properties of lanthanide-based nanocrystals: Crystal phase, lattice strain, downconversion, upconversion and energy transfer. *Nanoscale* **2012**, *4*, 3608–3619.

[24] Chen, F.; Bu, W.; Zhang, S.; Liu, J.; Fan, W.; Zhou, L.; Peng, W.; Shi, J. Gd^{3+}-ion-doped upconversion nanoprobes: Relaxivity mechanism probing and sensitivity optimization. *Adv. Funct. Mater.* **2013**, *23*, 298–307.

[25] Johnson, N. J. J.; Oakden, W.; Stanisz, G. J.; Prosser, R. S.; van Veggel, F. C. J. M. Size-tunable, ultrasmall $NaGdF_4$ nanoparticles: Insights into their T_1 MRI contrast enhancement. *Chem. Mater.* **2011**, *23*, 3714–3722.

[26] Dong, C.; Korinek, A.; Blasiak, B.; Tomanek, B.; van Veggel, F. C. J. M. Cation exchange: A facile method to make $NaYF_4$:Yb,Tm–$NaGdF_4$ core–shell nanoparticles with a thin, tunable, and uniform shell. *Chem. Mater.* **2012**, *24*, 1297–1305.

[27] Cheng, L.; Wang, C.; Liu, Z. Upconversion nanoparticles and their composite nanostructures for biomedical imaging and cancer therapy. *Nanoscale* **2013**, *5*, 23–37.

[28] Liu, J.; Bu, W.; Pan, L.; Shi, J. NIR-triggered anticancer drug delivery by upconverting nanoparticles with integrated azobenzene-modified mesoporous silica. *Angew. Chem. Int. Edit.* **2013**, *52*, 4375–4379.

[29] Wang, G.; Peng, Q.; Li, Y. Lanthanide-doped nanocrystals: Synthesis, optical-magnetic properties, and applications. *Acc. Chem. Res.* **2011**, *44*, 322–332.

[30] Li, X.; Shen, D.; Yang, J.; Yao, C.; Che, R.; Zhang, F.; Zhao, D. Successive layer-by-layer strategy for multi-shell epitaxial growth: Shell thickness and doping position dependence in upconverting optical properties. *Chem. Mater.* **2013**, *25*, 106–112.

[31] Li, Z. Q.; Zhang, Y. An efficient and user-friendly method for the synthesis of hexagonal-phase $NaYF_4$:Yb,Er/Tm nanocrystals with controllable shape and upconversion fluorescence. *Nanotechnology* **2008**, *19*, 345606.

[32] Pichaandi, J.; Boyer, J. C.; Delaney, K. R.; van Veggel, F. C. J. M. Two-photon upconversion laser (scanning and wide-field) microscopy using Ln^{3+}-doped $NaYF_4$ upconverting nanocrystals: A critical evaluation of their performance and potential in bioimaging. *J. Phys. Chem. C* **2011**, *115*, 19054–19064.

[33] Johnson, N. J. J.; Korinek, A.; Dong, C.; van Veggel, F. C. J. M. Self-focusing by ostwald ripening: A strategy for layer-by-layer epitaxial growth on upconverting nanocrystals. *J. Am. Chem. Soc.* **2012**, *134*, 11068–11071.

[34] Komban, R.; Klare, J. P.; Voss, B.; Nordmann, J.; Steinhoff, H. J.; Haase, M. An electron paramagnetic resonance spectroscopic investigation on the growth mechanism of $NaYF_4$:Gd nanocrystals. *Angew. Chem. Int. Edit.* **2012**, *51*, 6506–6510.

[35] Mai, H. X.; Zhang, Y. W.; Si, R.; Yan, Z. G.; Sun, L. D.; You, L. P.; Yan, C. H. High-quality sodium rare-earth fluoride nanocrystals: Controlled synthesis and optical properties. *J. Am. Chem. Soc.* **2006**, *128*, 6426–6436.

[36] Dou, Q. Q.; Idris, N. M.; Zhang, Y. Sandwich-structured upconversion nanoparticles with tunable color for multiplexed cell labeling. *Biomaterials* **2013**, *34*, 1722–1731.

[37] Abel, K. A.; Boyer, J. C.; Andrei, C. M.; van Veggel, F. C. J. M. Analysis of the shell thickness distribution on $NaYF_4$/$NaGdF_4$ core/shell nanocrystals by EELS and EDS. *J. Phys. Chem. Lett.* **2011**, *2*, 185–189.

[38] Abel, K. A.; Boyer, J. C.; van Veggel, F. C. J. M. Hard proof of the $NaYF_4$/$NaGdF_4$ nanocrystal core/shell structure. *J. Am. Chem. Soc.* **2009**, *131*, 14644–14645.

[39] Chen, G. Y.; Shen, J.; Ohulchanskyy, T. Y.; Patel, N. J.; Kutikov, A.; Li, Z. P.; Song, J.; Pandey, R. K.; Agren, H.; Prasad, P. N.; Han, G. (α-$NaYbF_4$:Tm^{3+})/CaF_2 core/shell nanoparticles with efficient near-infrared to near-infrared upconversion for high-contrast deep tissue bioimaging. *ACS Nano* **2012**, *6*, 8280–8287.

[40] Garcia-Gutierrez, D.; Gutierrez-Wing, C.; Miki-Yoshida, M.; Jose-Yacaman, M. HAADF study of Au–Pt core–shell bimetallic nanoparticles. *Appl. Phys. A* **2004**, *79*, 481–487.

[41] Zhang, F.; Che, R.; Li, X.; Yao, C.; Yang, J.; Shen, D.; Hu, P.; Li, W.; Zhao, D. Direct imaging the upconversion nanocrystal core/shell structure at the subnanometer level: Shell thickness dependence in upconverting optical properties. *Nano Lett.* **2012**, *12*, 2852–2858.

[42] van Veggel, F. C. J. M.; Dong, C. H.; Johnson, N. J. J.; Pichaandi, J. Ln^{3+}-doped nanoparticles for upconversion and magnetic resonance imaging: Some critical notes on recent progress and some aspects to be considered. *Nanoscale* **2012**, *4*, 7309–7321.

[43] Park, Y.; Kim, H. M.; Kim, J. H.; Moon, K. C.; Yoo, B.; Lee, K. T.; Lee, N.; Choi, Y.; Park, W.; Ling, D.; et al. Theranostic probe based on lanthanide-doped nanoparticles for simultaneous *in vivo* dual-modal imaging and photodynamic therapy. *Adv. Mater.* **2012**, *24*, 5755–5761.